Soft Matter

Toward Strong Self-Healing Polyisoprene Elastomers with Dynamic Ionic Crosslinks

Journal:	*Soft Matter*
Manuscript ID	SM-ART-01-2020-000058.R1
Article Type:	Paper
Date Submitted by the Author:	10-Feb-2020
Complete List of Authors:	Miwa, Yohei; Gifu University, Department of Chemistry and Biomolecular Science Kurachi, Junosuke; Gifu University, Department of Chemistry and Biomolecular Science Sugino, Yusuke; Gifu University, Department of Chemistry and Biomolecular Science Udagawa, Taro; Gifu University, Department of Chemistry and Biomolecular Science Kutsumizu, Shoichi; Gifu University, Department of Chemistry, Faculty of Engineering

ARTICLE

Toward Strong Self-Healing Polyisoprene Elastomers with Dynamic Ionic Crosslinks

Received 00th January 20xx,
Accepted 00th January 20xx

DOI: 10.1039/x0xx00000x

Yohei Miwa,*[a,b] Junosuke Kurachi,[a] Yusuke Sugino,[a] Taro Udagawa[a] and Shoichi Kutsumizu[a]

To compromise high mechanical strength and efficient self-healing capability in an elastomer with dynamic crosslinks, optimization of the molecular structure is crucial in addition to the tuning of the dynamic properties of the crosslinks. Herein, we studied the effects of molecular weight, content of carboxy groups, and neutralization level of ionically crosslinked polyisoprene (PI) elastomers on their morphology, network rearrangement behavior, and self-healing and mechanical properties. In this PI elastomer, nanosized sphere-shaped ionic aggregates are formed by both neutralized and non-neutralized carboxy groups that act as stickers. The number density of the ionic aggregates that act as physical crosslinks increased with increase in the stickers' concentration, although the size of the ionic aggregates was independent of the molecular weight and the stickers' concentration. The ionic network was dynamically rearranged by the stickers' hopping between the ionic aggregates, and the rearrangement was accelerated by decreasing the neutralization level. We found that the $2R_g$ of the PI must be significantly larger than the average distance between the ionic aggregates to obtain a mechanically strong PI elastomer. We also found that further increase in the molecular weight is effective to enhance the dimensional stability of the elastomer. However, this approach reduced the elastomer's self-healing rate at the same time because the diffusion and randomization of the polymer chains between the damaged faces were reduced. In this work, we clearly demonstrated the principle in the optimization of the molecular structure for the ionically crosslinked PI elastomers to tune the mechanical and autonomous self-healing properties.

Introduction

Recently, elastomers consisting of reversible rubber network crosslinked with dynamic bonds, such as dynamic covalent bonds[1–18], hydrogen bonding[19–29], π–π interaction[30], ionic interaction[21,31–44], host–guest chemistry[45,46], metal–ligand interaction[46–53] have received considerable attention. Because of the dynamic nature of the bonds that spontaneously associate and disassociate at ambient or specific conditions, dynamically crosslinked elastomers exhibit unique behaviors such as self-healing, enhanced fatigue, fracture resistance, and ultra-stretchability. Recently, several dynamically crosslinked elastomers that spontaneously self-heal after damage even at room temperature without inputs of external energy (such as heat or light) or healing agents (such as monomers, solvents, and catalysts) have been developed.[19,20,22–24, 26–29,31–35,37,39,42,48–53] Such autonomous self-healing properties are potentially useful for many advanced applications such as wearable devices and the skin of robots.[54–56] Although the overall mechanical performance of these materials is important for practical applications, such elastomers tend to be soft and viscoelastic because of the formation of weak dynamic bonds during crosslinking. Therefore, designing elastomers that spontaneously self-heal and exhibit high strength is necessary. Recently, a simple ionically crosslinked polyisoprene (PI) elastomer that demonstrated high fracture strength and spontaneously self-healed at room temperature was designed and developed by the authors.[37] Moderately modified polymers with ionic groups are generally called ionomers. In our study, unlike the previously reported telechelic PI ionomers[57-61], neutralized and non-neutralized carboxy groups which acted as stickers, were attached along the main chain of PI. Both the neutralized and non-neutralized carboxy groups formed small ionic aggregates that acted as physical crosslinks. However, stickers attached to the PI chains continually hopped between neighbouring ionic aggregates at room temperature, i.e., the crosslinked structure was not permanent because the network dynamically rearranged at room temperature. As the result of the network arrangement at room temperature, the ionic PI elastomer spontaneously healed after damage without healing agents or any input of external energy. Furthermore, the elastomer behaved as strong elastic material under rapid deformation; however, it switches to highly stretchable and viscoelastic material against slow deformation due to the network rearrangement.[37] Moreover, the self-healing rate and tensile property of the ionic elastomer was easily tunable by the neutralization level of the carboxy groups because of the network rearrangement rate that increased with decreasing the neutralization level. Additionally, the molecular weight of the PI

[a] Department of Chemistry and Biomolecular Science, Faculty of Engineering, Gifu University, Yanagido, Gifu 501-1193, Japan.
[b] PRESTO, Japan Science and Technology Agency.
† Electronic Supplementary Information (ESI) available: Supporting data such as FT-IR and DFT calculations. See DOI: 10.1039/x0xx00000x

backbone and sticker concentration must be important parameters to finely optimize the network rearrangement and the mechanical properties of the elastomer. In this study, we focus on the effects of the molecular weight and sticker concentration of the ionically crosslinked PI elastomer based on the network rearrangement, self-healing rate, and mechanical properties.

Experiments

Sample preparation

Materials. Isoprene (>99%) and N,N,N',N'-tetramethylethylenediamine (TMEDA, >98%) were purchased from Tokyo Chemical Industry Co., Ltd. *sec*-Butyllithium (*sec*-BuLi, 1 mol L^{-1} in cyclohexane (95%) and *n*-hexane (5%)), cyclohexane (extra-pure reagent), tetrahydrofuran (THF, extra-pure reagent), methanol (extra-pure reagent), hydrochloric acid (HCl, 35%), and $CDCl_3$ (99.8%) were obtained from Nacalai Tesque, Inc. and used without further purification. Molecular sieves (3A 1/16, Nacalai Tesque) and aluminium oxide (activated, Kanto Chemical Co., Inc.) were dried before use.

Polymerization of PI. The PI was synthesized via living anionic polymerization using *sec*-BuLi as an initiator.[37] We determined the number average molecular weight (M_n) and molecular weight distribution (M_w/M_n) by gel permeation chromatography (GPC). We prepared three narrow polydispersed PIs having different molecular weights: PI1 (M_n = 12,400 Da, M_w/M_n = 1.05), PI2 (M_n = 96,900 Da, M_w/M_n = 1.04), and PI3 (M_n = 500,000 Da, M_w/M_n = 1.22). We used ^{13}C-NMR spectroscopy to confirm the microstructure composition of the PIs: PI1 (76% *cis*-1,4; 18% *trans*-1,4; and 6% 3,4 microstructures); PI2 (76% *cis*-1,4; 18% *trans*-1,4; and 6% 3,4 microstructures); and PI3 (75% *cis*-1,4; 18% *trans*-1,4; and 7% 3,4 microstructures).

Preparation of ionically modified PI. The ionically modified PI was prepared according to Scheme 1.[37] The concentration of the carboxy groups attached to the PI main chain was controlled by the amount of *sec*-BuLi and TMEDA added to the PI/cyclohexane solution under N_2 flow. The reaction was terminated via bubbling dry CO_2 gas (99.9%). The reaction mixture was then dissolved in THF and poured into methanol, followed by the isolation of the precipitate. The precipitate was then dissolved in THF, and then aqueous HCl was added until the solution became acidic. The mixture was then poured into excess methanol and the final product was precipitated. The resultant carboxylic PI (PI-COOH) was dried under vacuum at 45 °C for >3 days. We determined the actual concentration of carboxy groups in the PI via Fourier-transform infrared (FT-IR) spectroscopy using references (mixtures of PI and lauric acid).[37] In this study, the degree of neutralization with NaOH was typically controlled between 85% and 90% using the following procedure. In brief, an appropriate amount of NaOH/methanol solution (3.9 g L^{-1}) was slowly added to a carboxylic PI/THF solution (10 wt%) with vigorous stirring. The viscosity of the solution increased because of the neutralization of the carboxy groups. The mixture was then poured into a Teflon petri dish and dried at 35 °C to produce a cast film, which was further dried under vacuum at 35 °C for >1 day. The thickness of the cast films was ~0.4 mm. By neutralization, the intensity of the stretching vibration of the carbonyl of COOH in the FT-IR band decreased at 1707 cm^{-1} while an asymmetric stretching vibration band of sodium carboxylate was observed at 1590 cm^{-1} (Fig. S1). The actual degree of neutralization was determined from the reduction of the band intensity at 1707 cm^{-1}, which was normalized by the band intensities of the C=C stretching vibrations at 1665 and 1644 cm^{-1}. The molecular weights of COOH concentration and the degree of neutralization with sodium in the prepared samples are listed in Table 1.

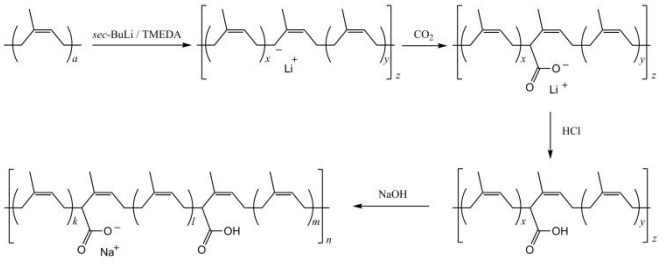

Scheme 1. Ionic modification of PI.

Table 1. Characteristics of prepared samples.

Notation	M_n[a]	M_w/M_n[a]	COOH[b] / mol%	Na[c] / %
PI1	12,400	1.05	N/A	N/A
PI1(1.2)66Na			1.2	66
PI1(1.2)85Na			1.2	85
PI1(2.5)86Na			2.5	86
PI2	96,900	1.04	N/A	N/A
PI2(0.4)88Na			0.4	88
PI2(1.4)85Na			1.4	85
PI2(2.7)58Na			2.7	58
PI2(2.7)90Na			2.7	90
PI3	500,000	1.22	N/A	N/A
PI3(0.7)88Na			0.7	88
PI3(1.6)90Na			1.6	90

[a]M_n and M_w/M_n were determined by GPC. [b]This value is related to the non-neutralized sample. [c]Degree of neutralization with NaOH determined by FT-IR.

Measurements. ^{1}H-NMR and ^{13}C-NMR spectra were obtained on JEOL-ECS400 (400 MHz) spectrometer. Prior to analysis, samples were dissolved in $CDCl_3$ and tetramethylsilane was used as an internal standard. The weight and number average molecular weights of PI were determined by GPC using an HLC-8020 apparatus (manufactured by Tosoh Co., Ltd.). Two polystyrene gel columns (Tosoh TSK gel GMH, G4000HXL and G2000HXL) were connected to an RI-4030 RI detector (JASCO). THF was used as the eluent at 40 °C. The column set was calibrated using standard monodisperse PI (Scientific Polymer Products) samples. FT-IR spectra were obtained with a Perkin-Elmer Spectrum400 spectrometer equipped with a DTGS detector. Prior to analysis, a thin sample film was prepared via press molding at 100 °C, while liquid samples were sandwiched between KBr plates. The thickness of the sample films was controlled to ensure that the absorbances of the bands obeyed the Lambert–Beer law. Measurements were performed in the transmittance mode at an optical resolution of 4 cm^{-1} using 32 scans. Tensile stress–strain curves of the sample films were collected using the AND Force Tester

MCT-2150 at 27 ± 1°C. Dumbbell-shaped tensile bars, with dimensions of 25 × 2.0 × 0.4 mm were cut from the cast films. The initial gauge length was set to 11 mm, and the stretching speed was selected in the range of 10–300 mm min^{-1}. Each measurement was performed at least three times. The tensile stress (σ) was calculated using $\sigma = F/S_0$, where S_0 is the initial cross-sectional area of the sample film and F is the loading force. The strain (ε) under elongation was defined as the marker distance (l) compared to the initial marker distance (l_0) of the specimen, i.e., $\varepsilon = (l - l_0)/l_0 \times 100\%$. The increasing marker distance was monitored by a video camera. The rheological properties were investigated in oscillatory shear mode on a parallel-plate rheometer (AR-G2, TA instruments) with 8 mm diameter plates. The thickness of the sample was ~0.4 mm, and a strain of 0.1% was applied. A temperature sweep test was performed at 1 Hz in the range between –100 and 150 °C at a heating rate of 3 °C min^{-1}. Frequency sweep tests were performed within a dynamic range of 0.01–100 Hz. Synchrotron SAXS measurements were performed using the BL-6A beam line at the Photon Factory of High Energy Accelerator Research Organization (KEK) in Tsukuba, Japan. The wavelength of the X-ray beam was 0.15 nm. A PILATUS-1M was used as the detector. The distance between the detector and sample position was 1 m. Stearic acid and silver behenate were used as the standards.

DFT Calculations. To estimate the interaction energy between the stickers, we performed density functional theory (DFT) calculations. To narrow down the numerous possible conformations for those with lower electronic energies, the global reaction route mapping (GRRM) method was explored for isoprene trimers modified with sodium carboxylate or carboxy groups. [62-66] The GRRM calculation was performed with a large-anharmonic downward distortion (LADD) = 3, NLowest = 20 and EQonly keywords. Also, the bond condition option was adopted to prevent covalent bonds in the given initial geometry from breaking. The initial geometry for GRRM calculation was obtained using a PM6 geometry-optimization calculation. The maximum covalent bond lengths were set to be 20% longer than the initial covalent bond lengths. The GRRM calculation was performed following the PM6 method in gas phase to produce 82 EQs, which were then used for DFT calculations (M06[67]/6-31G** with Int(grid=ultrafine) keyword). The 10 lowest-energy monomer conformations were used in building 55 initial geometries for the DFT calculation of a combination comprising isoprene trimers modified with carboxy groups. The interaction energy of COOH···HOOC was then calculated as the average interaction energy of the 10 lowest-energy combinations. The initial geometries for the DFT calculation of COOH···NaOOC and COONa···NaOOC combinations were obtained by replacing the H atom(s) in COOH group in the 10 lowest-energy combinations with Na atom(s). All calculations were performed using the GAUSSIAN09 Revision B.01 program package.[68]

Self-healing tests. Using a razor and a spacer, a sample film was cut, leaving a thickness of 12.5 μm, to avoid completely cutting the film into two separate pieces. The cut faces were then placed in contact. The sample films were stored at room temperature (27 ± 1 °C) for 64 h. The healed sample films were then stretched at 100 mm min^{-1} and 27 ± 1 °C. The self-healing efficiency was defined as the ratio between the areas below the stress–strain curves for the original and self-healed materials.

Results and Discussion

Characterization of ionic aggregates. Carboxy and sodium carboxylate groups aggregated with each other and formed ionic aggregates in the hydrophobic PI matrix. The ionic aggregates acted as physical crosslinks in the ionic elastomers. In this section, the effects of the molecular weight of PI and the concentration of stickers (carboxy and sodium carboxylate groups) on the size and number density of ionic aggregates are examined. SAXS profiles of ionized samples have a broad scattering peak, usually called the "ionomer peak" at q = 0.5–1.5 nm^{-1} ($q = (4\pi/\lambda)\sin\theta$)(Fig. 1(A)). The ionomer peak was a scattering from interference between ionic aggregates. The experimental scattering patterns simulated based on the Yarusso–Cooper model.[69] In this model, spherical particles, with an ionic core (having a radius of R_1) and a restricted hydrocarbon shell of a thickness of $R_{CA} - R_1$, randomly disperse with the closest approach limitation, $2R_{CA}$, for neighboring aggregates. The scattering intensity for this model is presented by

$$I(q) = K\frac{V_1^2}{V_p}\Phi(qR_1)^2\frac{1}{1+(\frac{8V_{CA}}{V_p})\Phi(2qR_{CA})} \quad (1)$$

$$V_{CA} = \frac{4}{3}\pi R_{CA}^3 \quad (2)$$

$$V_1 = \frac{4}{3}\pi R_1^3 \quad (3)$$

$$\Phi(x) = 3\frac{\sin x - x\cos x}{x^3} \quad (4)$$

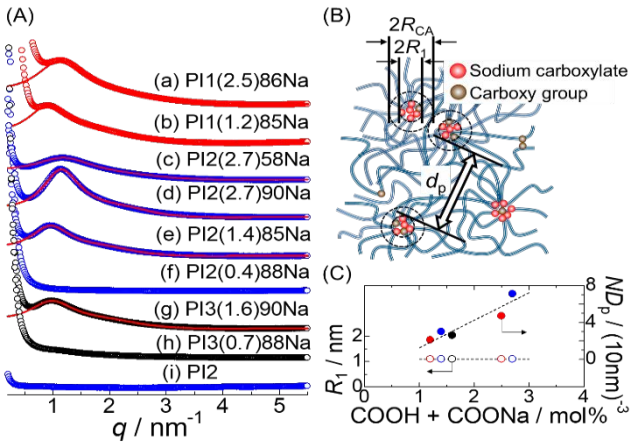

Fig. 1 (A) SAXS profiles for (a) PI1(2.5)86Na, (b) PI1(1.2)85Na, (c) PI2(2.7)58Na, (d) PI2(2.7)90Na, (e) PI(1.4)85Na, (f) PI2(0.4)88Na, (g) PI3(1.6)90Na, (h) PI3(0.7)88Na, and (i) PI2. Experimental and simulated data are shown with open circles and curves, respectively. (B) Schematic of R_1 and R_{CA}. The average distance between the ionic cores, d_p, is also displayed. (C) Plots of R_1 (open symbols) and ND_p (solid symbols) for the samples against sticker (carboxy and sodium carboxylate groups) concentration. Red, blue, and black symbols represent PI1-, PI2-, and PI3-based elastomers, respectively. The datum for PI2(2.7)58Na is omitted.

Table 2. Structural parameters for each sample analyzed by SAXS.

Sample	R_1 / nm	R_{CA} / nm	V_p / nm^3	ND_p / (10nm)$^{-3}$	d_p / nm	$2R_g$ / nm
PI1(2.5)86Na	1.1	2.3	210	4.7	5.2	7.0
PI1(1.2)85Na	1.1	2.9	470	2.1	7.4	7.0
PI2(2.7)58Na	1.0	2.1	220	4.5	5.3	20
PI2(2.7)90Na	1.1	2.4	140	7.1	4.2	20
PI2(1.4)85Na	1.1	2.8	330	3.0	6.4	20
PI3(1.6)90Na	1.1	2.7	380	2.6	6.8	45

R_1: the radius of the ionic core; R_{CA}: radius of the ionic core plus the hydrocarbon shell; V_p: the average sample volume occupied by one ionic core; ND_p: the number density of ionic core per (10 nm)^3; d_p: average distance between ionic cores.

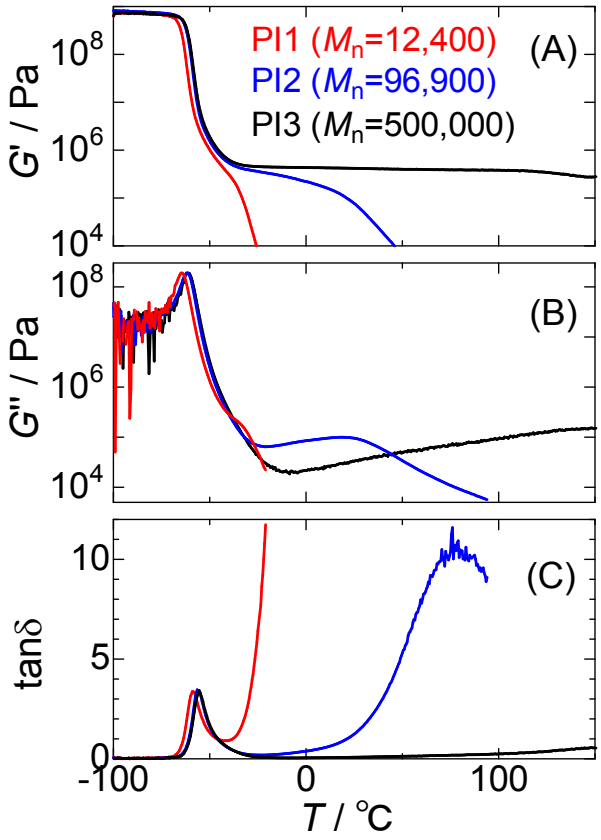

Fig. 2 Temperature dependence of (A) storage modulus (G'), (B) loss modulus (G''), and (C) tanδ for PI1, PI2, and PI3 measured at 1 Hz.

where V_p and K are the average sample volume occupied by one particle of ionic core and an adjustable parameter for scattering intensity, respectively. The sample values of R_1, R_{CA}, and V_p are listed in Table 2. The number density of the ionic aggregates (ND_p) and the average distance between ionic cores (d_p) are calculated from the V_p; these values are also listed in Table 2. When calculating the d_p, the sample volume occupied by an ionic core was simply assumed to be a sphere having a radius r, and the d_p was obtained from $2r - 2R_1$. The R_1, R_{CA}, and d_p are schematically depicted in Fig. 1(B). Furthermore, the R_1 and ND_p are plotted against the sticker concentration, as shown in Fig. 1(C). The value of R_1 was ~ 1 nm, irrespective of the PI molecular weight and the sticker concentration in the PI since the aggregation number of the stickers is limited by steric hindrances between the polymer chains around the ionic aggregates.[70] However, the ND_p increased by increasing the concentration of the stickers. In Table 2, a double value of the radius of gyration ($2R_g$) for the PI is listed. Here, the $2R_g$ was calculated for PI1, PI2, and PI3, which are PI homopolymers before ionic modification.[71] The d_p of PI1(2.5)86Na and PI1(1.2)85Na was comparable to $2R_g$, while the d_p was much smaller than $2R_g$ for the other samples. When $2R_g$ is much larger than d_p, a polymer chain would bridge between ionic aggregates. However, if $2R_g$ is comparable to d_p, the polymer chains bridging between the ionic aggregates would be minor, and the elastomer would be weak and brittle. The mechanical properties are discussed below.

Rheological property of the precursor PI homopolymers. Fig. 2 shows the temperature dependences of storage (G') and loss (G'') moduli and tanδ for PI1, PI2, and PI3 measured at 1 Hz. The glass transition temperature (T_g), defined as the peak temperature of the G'' for PI1, PI2, and PI3, were determined as –64.5 °C, –61.5 °C, and –61.1 °C, respectively. PI1 showed a slightly lower T_g than the other two because of its low molecular weight.[72] Nevertheless, the difference in these samples is very minimal. On the other hand, the plateau region in G' significantly increased with increase in the molecular weight. The plateau region in PI1 was negligible, which indicated that the entanglement in PI1 was minimal, while considerable entanglement existed in PI3 because of its large molecular weight.

Effect of sticker concentration on ionic network rearrangement. Fig. 3 shows the comparison of the rheological results for PI2 and PI2-based ionic elastomers. Following ionic modification, there was a slight increase in the T_g. This increase was attributed to the restriction of segmental motion of the PI chain because of ionic modification whose effect was minimal. Moreover, the plateau in G' significantly extended toward high temperatures because of ionic modification. Furthermore, the presence of new relaxation for PI2(1.4)85Na, PI2(2.7)90Na, and PI2(2.7)58Na was observed in the range from −10 to 50 °C. As described in our previous study, this relaxation was ascribed to the hopping motion of the stickers between neighboring ionic aggregates,[37] which is generally called "ion-hopping."[73–75] During this motion, the neutralized and non-neutralized carboxy groups hop between neighboring ionic aggregates together with the attached polymer chains. Consequently, a network rearrangement was generated. The transient crosslinking in ionomers with ion-hopping provides unique viscoelastic behavior; the behavior has been

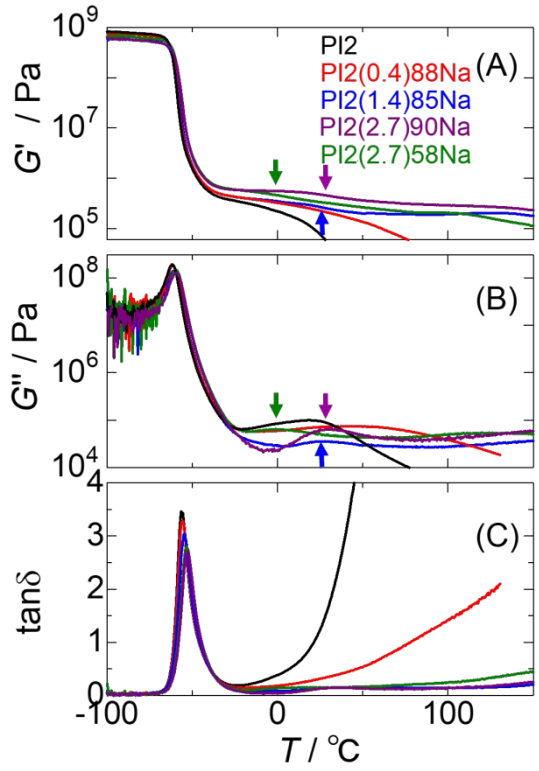

Fig. 3 Temperature dependences of (A) storage modulus (G'), (B) loss modulus (G''), and (C) tanδ for PI2, PI2(0.4)88Na, PI2(1.4)85Na, PI2(2.7)90Na, and PI2(2.7)58Na measured at 1Hz. Blue, purple, and green arrows indicate a relaxation temperature assigned to the exchange of ionic network for PI2(1.4)85Na, PI2(2.7)90Na, and PI2(2.7)58Na, respectively.

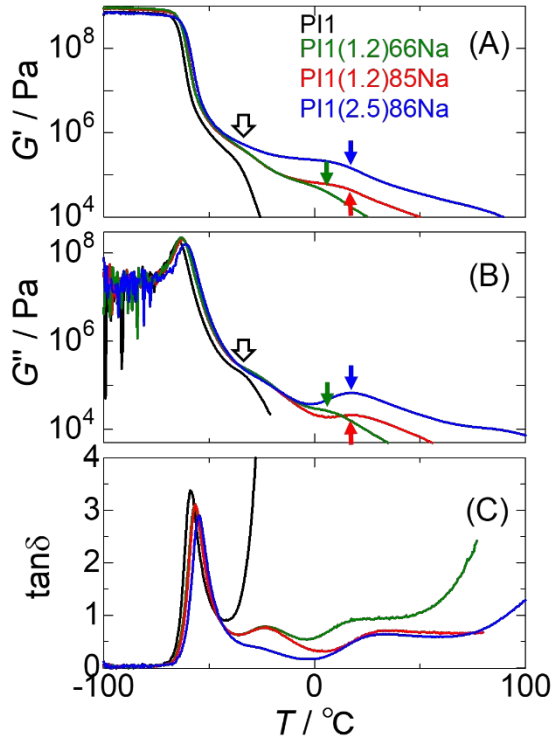

Fig. 4 Temperature dependences of (A) storage modulus (G'), (B) loss modulus (G''), and (C) tanδ for PI1, PI1(1.2)66Na, PI1(1.2)85Na, and PI1(2.5)86Na obtained at 1 Hz. Green, red, and blue arrows indicate a relaxation temperature assigned to the ionic network rearrangement for PI1(1.2)66Na, PI1(1.2)85Na, and PI1(2.5)86Na, respectively. Open arrow indicates the flow temperature of the unmodified PI component.

theoretically and experimentally studied.[43,77-83] The relaxation temperatures, defined as the G'' peak for PI2(1.4)85Na, PI2(2.7)90Na, and PI2(2.7)58Na, were determined as 26 °C, 28 °C, and –1.0 °C, respectively. This relaxation was not apparent for PI2(0.4)88Na because of its low sticker concentration. From comparison between PI2(2.7)90Na and PI2(2.7)58Na, a decrease in the degree of neutralization significantly accelerated the rearrangement of the ionic network as previously reported.[37] This was because of the plasticization effect of the non-neutralized carboxy groups in the ionic aggregates, which weakened ionic aggregation and accelerated ion hopping.[72-75] However, the difference in the relaxation temperatures of PI2(1.4)85Na and PI2(2.7)90Na was very minimal, although the concentration of the stickers was considerably different. This indicated that the concentration of the stickers does not affect the network rearrangement rate, at least in this concentration range. If the concentration of the stickers was significantly increased, the network rearrangement would appear to be restricted. Fig. 4 shows the rheological results for PI1, PI1(1.2)66Na, PI1(1.2)85Na, and PI1(2.5)86Na. The T_gs of the ionized PI1 increased by a few degrees compared to normal PI1. This was attributed to the sticker interactions that consequently restricted segmental motion of PI. In addition to the glass transition temperature, the ionically modified PI1 exhibited an additional relaxation, which was ascribed to the rearrangement of the ionic network in the range of 0–50 °C. The relaxation temperatures, defined as G'' peak, for PI1(1.2)85Na, PI1(2.5)86Na, and PI1(1.2)66Na were obtained as 18 °C, 18 °C, and 9 °C, respectively. Similar to the results for the ionically modified PI2 shown in Fig. 3, the network rearrangement rate was insensitive to the sticker concentration; however, the decrease in the degree of neutralization remarkably accelerated the network rearrangement. Furthermore, the ionically modified PI1 exhibited a small relaxation at around –30 °C. This relaxation was related to the flow of the unmodified PI components in the samples. Because of the short chain length, some PI chains were not ionically modified.

Effect of molecular weight on ionic network rearrangement. Fig. 5 shows the comparison of the rheological results of PI1(1.2)85Na, PI2(1.4)85Na, and PI3(1.6)90Na. Their molecular weights were largely different from each other, but the sticker concentrations and the degree of neutralization for these samples were comparable with each other. The T_gs of PI1(1.2)85Na, PI2(1.4)85Na, and PI3(1.6)90Na were determined as −63 °C, −60 °C, and −60 °C, respectively. However, PI1(1.2)85Na showed a slightly lower T_g compared to PI2(1.4)85Na and PI3(1.6)90Na because of its low molecular weight. The relaxation temperatures ascribed to the ionic network rearrangement for PI1(1.4)85Na, PI2(1.4)85Na, and PI3(1.6)90Na

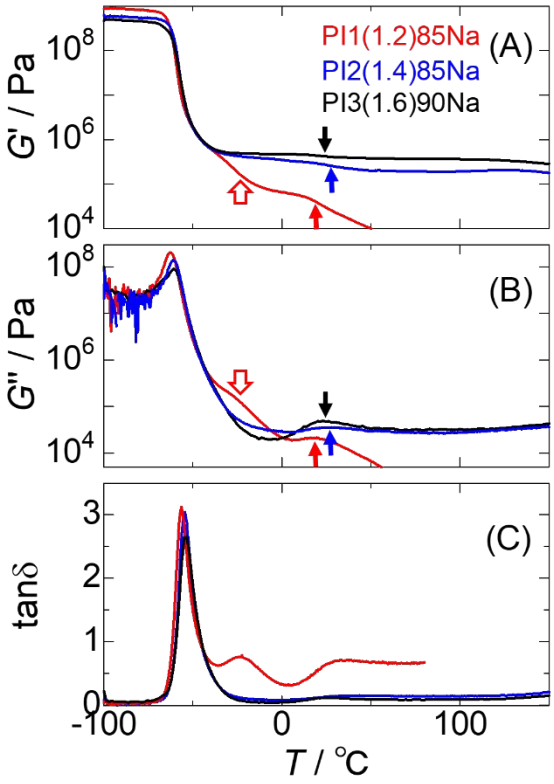

Fig. 5 Temperature dependences of (A) G', (B) G'', and (C) tanδ for PI1(1.2)85Na, P2(1.4)85Na, and PI3(1.6)90Na measured at 1 Hz. Red, blue, and black arrows indicate a relaxation temperature assigned to the ionic network rearrangement for PI1(1.2)85Na, PI2(1.4)85Na, and PI3(1.6)90Na, respectively. Open arrow indicates flow temperature of unmodified PI component.

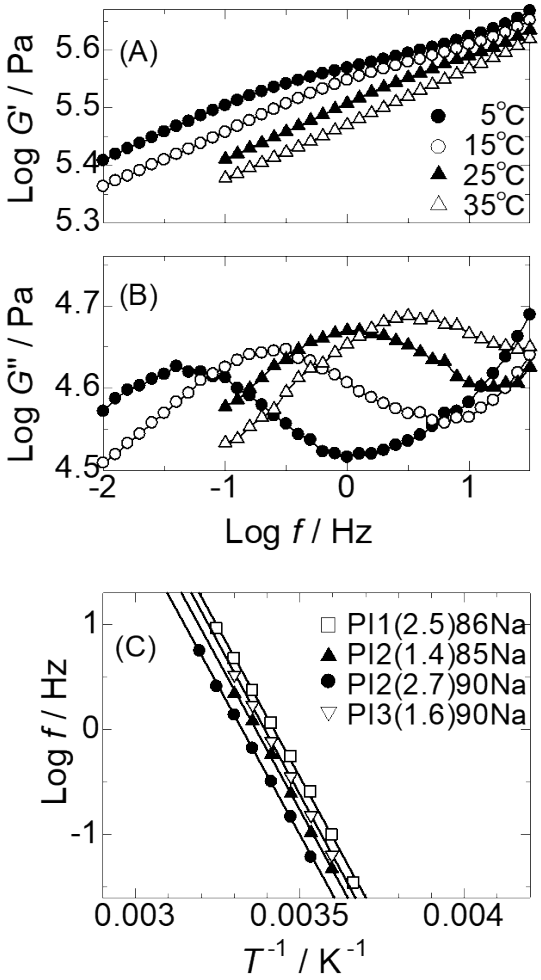

Fig 6. Frequency dependences of (A) G' and (B) G'' for P2(1.4)85Na at indicated temperatures. (C) The temperature dependences of ionic network rearrangement motion for the indicated samples.

were obtained at 18 °C, 26 °C, and 24 °C, respectively. PI2(1.4)85Na and PI3(1.6)90Na showed almost the same relaxation temperature, although the difference in their M_n was considerable. However, PI1(1.2)85Na showed a slightly lower relaxation temperature compared to others because of its low molecular weight. As described in the next section, the segmental motion of the PI chain was the driving force of the ionic network rearrangement. Therefore, if the M_n was very small, the relaxation temperature assigned to the ionic network rearrangement would significantly be decreased.

Origin of ionic network rearrangement. Our result was that the effects of the molecular weight and the sticker concentrations on the ionic network rearrangement were very minimal for the studied samples. Despite the large difference in the molecular weight, the relaxation temperatures assigned to the ionic network rearrangement for PI2(1.4)85Na and PI3(1.6)90Na were almost the same. This result demonstrated that the network rearrangement occurred at the segmental scale of the PI chain. Moreover, the driving force of the network rearrangement was because of the segmental mobility of the PI chain that was thermally activated. Therefore, the rearrangement of the ionic network was accelerated when the aggregation force between the stickers was weakened by decreasing the neutralization level. Fig.s 6(A) and 6(B) show the frequency dependence of G' and G'' for the ionic network rearrangement in PI2(1.4)85Na, respectively.

Moreover, the temperature dependences of the ionic network rearrangement in the samples is demonstrated in Fig. 6(C). The activation energies (E_as) for PI1(2.5)86Na, PI2(1.4)85Na, PI2(2.7)90Na, and PI3(1.6)90N, were determined as equal 111, 110, 109, and 111 kJ mol^{-1}, respectively. The E_as of these samples were almost equal irrespective of their different molecular weights and sticker concentrations. Elfadl et al. reported the temperature dependence of the segmental mobility of PI homopolymers in a very wide temperature range using dielectric spectroscopy and NMR.[72,84] The E_a for the segmental motion of the PI homopolymer with molecular weight of 157,000 Da was 66 kJ mol^{-1} in the range of 20–80 °C. Compared to the previously reported PI homopolymer, the ionically modified PI in this study exhibited much higher E_as because of the attractive interaction between the stickers, which restricted segmental motion of the PI chains.

As a further investigation on the mechanism of the ionic network rearrangement, interaction energies for the model combinations comprising isoprene trimers modified with sodium carboxylate or carboxy groups were calculated using the DFT method; the interaction

energy for the three combinations is listed in Table 3. Fig. S2 shows the chemical structure for the isoprene trimers used for the calculation and the molecular model for a particular combination with lowest energy. The interaction energy for COONa···NaOOC was the largest among the three combinations, which clearly indicated that the presence of the non-neutralized carboxy groups in the ionic aggregate weakened the sticker interactions. Consequently, the ionic network rearrangement was accelerated by decreasing the neutralization level. A similar conclusion was reported by Tierney and Register for poly(ethylene-*co*-methacrylic acid) ionomers based on cation diffusion measurement.[75] They further demonstrated that both the neutralized and non-neutralized carboxy groups diffuse in the poly(ethylene-*co*-methacrylic acid) ionomers. Though there has been no experimental evidence to date, we expect that both carboxy and sodium carboxylate groups hop between the ionic aggregates in our ionic PI elastomers.

Table 3. Interaction energy for three combinations calculated by DFT method.

Combination	Interaction Energy / kJ mol^{-1}
-COOH···HOOC-	−83
-COOH···NaOOC-	−133
-COONa···NaOOC-	−184

Effect of sticker concentration on tensile behavior. Tensile stress–strain curves for the ionically modified PIs with various molecular weights and sticker concentrations measured at 27 ± 1 °C and 100 mm min^{-1} are shown in Fig. 7. PI2(0.4)88Na exhibited a very weak strength, which is attributed to its low sticker interactions. However, PI2(1.4)85Na and PI2(2.7)90Na demonstrate much higher fracture stress than PI2(0.4)88Na. Moreover, PI2(2.7)90Na exhibited higher fracture stress and lower fracture strain compared to PI2(1.4)85Na because of the presence of higher number density of ionic aggregates (ND_p). As listed in Table 2, the ND_p for PI2(2.7)90Na was nearly double that of PI2(1.4)85Na. This result indicated that increase in the sticker concentration typically enhanced the mechanical strength of the elastomer because of the ionic aggregates acting as physical crosslinks. Similarly, PI3(1.6)90Na showed a higher fracture stress than the PI3(0.7)88Na. Moreover, the upturn in the stress–strain curve is observed at high strain for the samples with high sticker concentration. This is probably due to the strain-induced crystallization.[76] In fact, the ionically modified PI becomes opaque when the specimen is stretched as described in our previous paper.[37]

Effect of molecular weight on tensile behavior. As discussed above, the tensile strength depended on the sticker concentrations because of the ionic aggregates acting as physical crosslinks. However, despite the high sticker concentration, PI1(2.5)86Na demonstrated only brittle property (Fig. 7). As described above, d_p and $2R_g$ were comparable to each other for PI1(2.5)86Na. Note that the bridging chains between the ionic aggregates were minimal, which might be related to the brittleness of PI1(2.5)86Na. Therefore, a relatively large molecular weight was necessary for synthesizing this elastomer to generate high strength. From this viewpoint, the molecular weight of PI2 and PI3 was large enough because their $2R_g$s were much larger than the d_ps for elastomers (Table 2). The fracture stresses for PI2(1.4)86Na and PI3(1.6)90Na were comparable with each other, however,

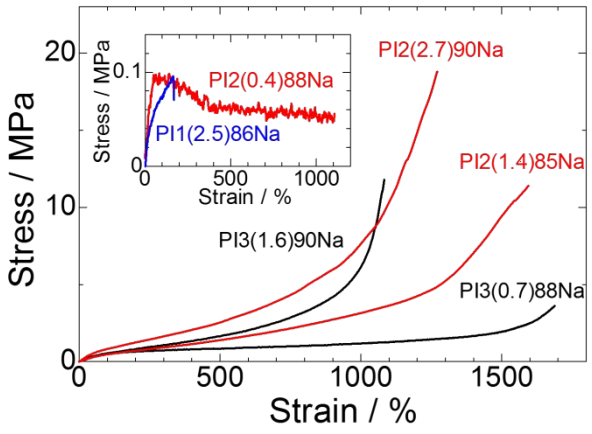

Fig. 7 Tensile stress–strain curves for the indicated samples. The measurement was performed at 100 mm min^{-1} and 27 ± 1 °C.

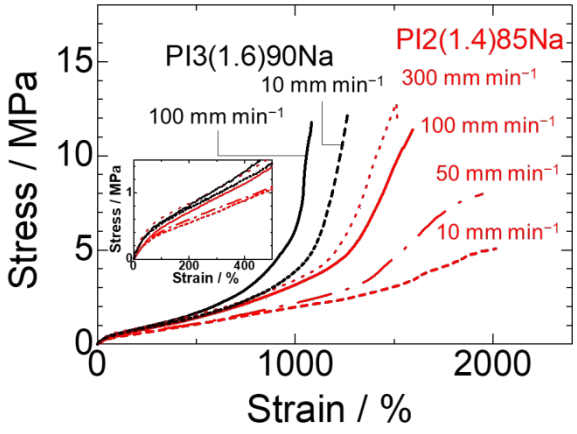

Fig. 8 Tensile stress–strain curves for PI2(1.4)85Na and PI3(1.6)90Na at indicated speed. The measurement was performed at 27 ± 1 °C.

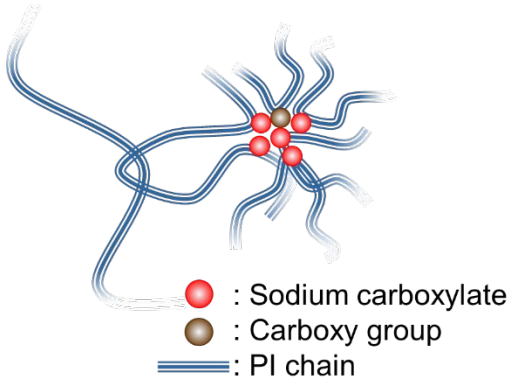

Fig. 9 Schematic of entanglement trapped by stickers.

PI3(1.6)90Na showed lower fracture strain than PI2(1.4)85Na. We consider that this was because of entanglement, which restricted the stretching of the sample. As discussed above, the entanglement in PI3

was much larger than that in PI2 because of its high molecular weight. The entanglement was further examined below. Fig. 8 shows the tensile stress–strain curves for PI2(1.4)85Na and PI3(1.6)90Na obtained at different stretching speeds. As previously reported, the tensile property of the ionically modified PI with a molecular weight of approximately 100,000 Da depends on the stretching speed, balanced with the rearrangement of the ionic network.[37] When the ionically modified PI was rapidly deformed it behaved like a strong elastic material. However, the sample acted like a stretchable and viscoelastic material under slow deformation. PI2(1.4)85Na was observed to behave in this manner, but the tensile behavior of PI3(1.6)90Na was insensitive to the stretching speed, although the ionic network rearrangement occurred at room temperature. After ionic modified of PI, some entanglements were considered to have been trapped by stickers, as shown in Fig. 9.[58] To release the trapped entanglement, the hopping of the trapping stickers to another ionic aggregate was necessary. Therefore, the release of the trapped entanglement was less operative compared to the rearrangement of the ionic network. Consequently, the stretchable and viscoelastic deformation of PI3(1.6)90Na was prevented even under stretching at 10 mm min^{-1}. However, PI3(1.6)90Na would behave as a stretchable material under very slow deformation.

Creep property. The creep behaviors of PI2(1.4)85Na, PI2(2.7)90Na, and PI3(1.6)90Na measured under a stress of 100 kPa at 30 °C are shown in Fig. 10. For PI2(1.4)85Na, the strain rate was 0.65% h^{-1} under a constant stress of 100 kPa. Furthermore, 14 h after the release, 5% of the strain remained. Because of the network rearrangement, PI2(1.4)85Na was slowly stretched under constant stress with a relatively large residual strain. However, it was deduced that the increase in sticker concentration and molecular weight was effective for stabilizing the specimen's dimension. For example, the strain rate and the residual strain for PI2(2.7)90Na were 0.21% h^{-1} and 3%, respectively. These values were approximately half that of PI2(1.4)85Na because of its larger number density of ionic aggregates, which contributed to the restricted diffusion of the PI chains compared to that of PI2(1.4)85Na. Moreover, the strain rate and the residual strain of PI3(1.6)90Na were 0.13% h^{-1} and 1%, respectively. PI3(1.6)90Na showed the best dimensional stability among the three samples. This result demonstrated that the trapped entanglement efficiently works for the dimensional stability of the ionically modified elastomers. The reduction of polymer chain diffusion based on molecular weight and sticker concentration was theoretically predicted by Leibler et al. [77]

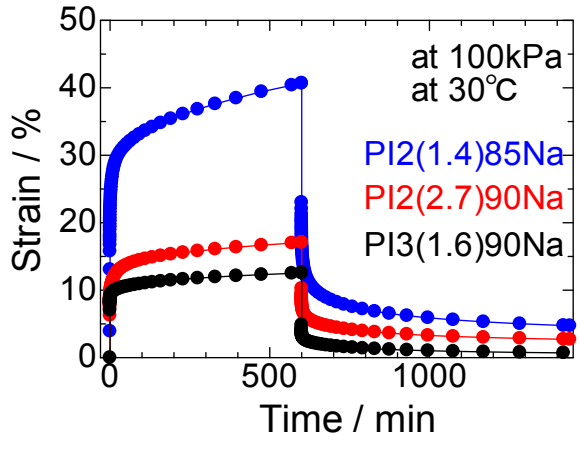

Fig. 10 Tensile creep results for PI2(1.4)85Na PI2(2.7)90Na, and PI3(1.6)90Na at 30 °C. A constant stress of 100 kPa was applied for 10 h and relaxed for 14 h.

Autonomous self-healing behavior. As shown in Fig. 11(A), the ionically modified PI exhibited autonomous self-healing behavior at room temperature. When a heart-shaped PI2(1.4)85Na film was cut, placed in contact, and healed at 27 ± 1 °C, the cut pieces were connected. Fig. 11(B) shows the tensile stress–strain curves for PI2(1.4)85Na, PI2(2.7)90Na, and PI3(1.6)90Na self-healed at 27 ± 1 °C for 64 h. The stress–strain curves of the initial specimen are also displayed in the same figure. Unlike the high fracture stress for the healed PI2(1.4)85Na, those for the healed PI(2.7)90Na and PI3(1.6)90Na were <2 MPa. The self-healing efficiencies for the PI2(1.4)85Na, PI2(2.7)90Na, and PI3(1.6)90Na are compared in Fig. 11(C). Here, the self-healing efficiency was calculated as the ratio between the areas below the stress–strain curves for the original and self-healed materials. Fig. 11(C) clearly demonstrates that an increase in the sticker concentration and molecular weight reduced the self-healing rate. Furthermore, as shown in Fig. 6, the rates of the ionic network rearrangement in the segmental scale were almost the same for these samples. However, the diffusion of the polymer chains was reduced by the increases in the molecular weight and the sticker concentration. Both diffusion and randomization of polymer chains

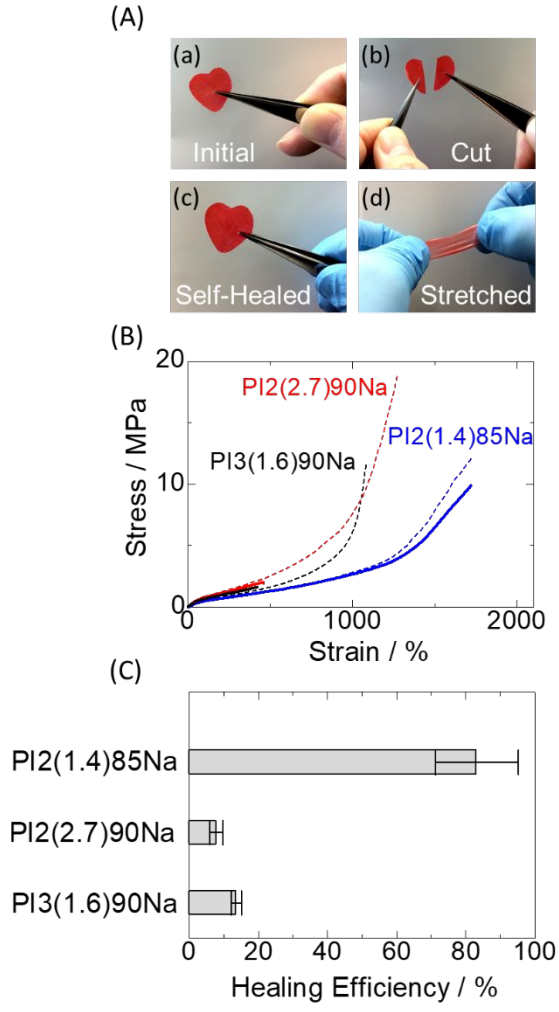

Fig. 11 (A) Images of self-healing behavior of heart-shaped PI2(1.4)85Na film at 27 ± 1 °C. The film was painted red. Images (a), (b), and (c) show initial, cut, and self-healed states, respectively, while (d) shows that the self-healed film was stretched. (B) Tensile stress–strain curves for original (broken) and self-healed (solid) PI2(1.4)85Na, PI2(2.7)90Na, and PI3(1.6)90Na. The samples were healed at 27 ± 1 °C for 64 h. (C) Healing efficiency of PI2(1.4)85Na, PI2(2.7)90Na, and PI3(1.6)90Na healed at 27 ± 1 °C for 64 h.

between the damaged faces were necessary to fully recover the strength as suggested by Wool et al.[85] To conclude, increasing both the sticker concentration and molecular weight was effective to enhance the mechanical strength and dimensional stability of the ionically modified PI. However, this approach reduced the self-healing rate at the same time. Further studies to overcome this limitation are currently underway and will be reported soon.

Conclusions

In this work, ionically modified PIs with different molecular weights and sticker concentrations were prepared to investigate the effects of the molecular structures on the morphology, the network rearrangement behavior, self-healing rate, and mechanical properties of the elastomer. The following insights were obtained. The size of the ionic aggregates that acted as the physical crosslinks were independent of the molecular weight and concentration of the stickers (sodium carboxylate and carboxy groups) in the ionic PI elastomer. However, the number density of the ionic aggregate increased with an increase in the sticker concentration but was independent of molecular weight. When the $2R_g$ of PI was much larger than the average distance between the ionic aggregates, the elastomer was mechanically strong because of the presence of several polymer chain bridges between the ionic aggregates. As for the network rearrangement behavior, the effects of the molecular weight and sticker concentration were minimal because the network rearrangement occurred in the segmental scale. However, the ionic network rearrangement was accelerated by decreasing the neutralization level because the presence of the non-neutralized carboxy groups in the ionic aggregates reduced the sticker interactions as demonstrated by DFT calculations. When the neutralization levels of the specimens were almost the same, the increases in the sticker concentration and molecular weight strengthened the mechanical properties of the elastomer. However, the self-healing rate decreased with increases in the molecular weight and sticker concentration, attributed to the diffusion and randomization of the polymer chains between the damaged faces that were reduced. In conclusion, we clearly demonstrated the effects of the molecular weight, content of carboxy groups, and neutralization level of the ionically crosslinked PI elastomers on their morphology, the network rearrangement behavior, and self-healing and mechanical properties. The obtained principle in the optimization of the molecular structure is crucial for the ionically crosslinked elastomers to tune their mechanical and autonomous self-healing properties.

Conflicts of interest

There are no conflicts to declare.

Acknowledgements

Beam time at PF-KEK provided by Programs 2016G627, 2017G562, and 2019G116 is acknowledged herein. Portion of these DFT calculations was performed at the Research Center for Computational Science (RCCS), Okazaki. This research was financially supported by the Japan Society for the Promotion of Science (Grant-in-Aid for Young Scientists (B), 16K17958 (YM), and Scientific Research (C), 18K05028 (TU) and 19K05612 (YM)); JST, PRESTO Grant Number JPMJPR199B(YM), Japan; The Mazda Foundation (17kk-079); The Ogasawara Foundation for the Promotion of Science & Engineering; and The Koshiyama Foundation.

Notes and references

1 X. Chen, M. A. Dam, K. Ono, A. Mal, H. Shen, S. R. Nutt, K. Sheran and F. Wudl, *Science* 2002, **295**, 1698–1702.
2 X. Chen, F. Wudl, A. K. Mal, H. Shen and S. R. Nutt, *Macromolecules* 2003, **36**, 1802–1807.
3 N. Yoshie, M. Watanabe, H. Araki and K. Ishida, *Polym. Degrad. Stab.* 2010, **95**, 826–829.
4 D. Montarnal, M. Capelot, F. Tournilhac and L. Leibler, *Science* 2011, **334**, 965–968.
5 J. Canadell, H. Goosens and B. Klumperman, *Macromolecules* 2011, **44**, 2536–2541.
6 Y. Amamoto, J. Kamada, H. Otsuka, A. Takahara and K. Matyjaszewski, *Angew. Chem. Int. Ed.* 2011, **50**, 1660–1663.
7 K. Imato, M. Nishihara, T. Kanehara, Y. Amamoto, A. Takahara and H. Otsuka, *Angew. Chem. Int. Ed.* 2012, **51**, 1138–1142.
8 C. Zeng, H. Seino, J. Ren, K. Hatanaka and N. Yoshie, *Macromolecules* 2013, **46**, 1794–1802.
9 C. Zeng, H. Seino, J. Ren, K. Hatanaka and N. Yoshie, *Polymer* 2013, **54**, 5351–5357.
10 H. Ying, Y. Zhang and J. Cheng, *Nat. Commun.* 2014, **5**, 3218.
11 K. Imato, T. Ohnishi, M. Nishihara, A. Takahara and H. Otsuka, *J. Am. Chem. Soc.* 2014, **136**, 11839–11845.
12 S. Ji, W. Cao and H. Xu, *Adv. Mater.* 2015, **27**, 7740–7745.
13 J. J. Cash, T. Kubo, A. Bapat and B. S. Sumerlin, *Macromolecules* 2015, **48**, 2098–2106.
14 M. Arslan, B. Kiskan and Y. Yagci, *Sci. Rep.* 2017, **7**, 5207.
15 W. A. Ogden and Z. Guan, *J. Am. Chem. Soc.* 2018, **140**, 6217–6220.
16 Y. Chen, Z. Tang, X. Zhang, Y. Liu, S. Wu and B. Guo, *ACS Appl. Mater. Interfaces* 2018, **10**, 24224–24231.
17 R. Bui and M. A. Brook, *Polymer* 2019, **160**, 282–290.
18 Y. Chen, Z. Tang, X. Zhang, Y. Liu, S. Wu and B. Guo, *Macromolecules* 2019, **52**, 3805–3812.
19 P. Cordier, F. Tournilhac, C. Soulie-Ziakovic and L. Leibler, *Nature* 2008, **451**, 977–980.
20 Y. Chen, A. M. Kushner, G. A. Williams and Z. Guan, *Nat. Chem.* 2012, **4**, 467–472.
21 A. Noro, M. Hayashi and Y. Matsushita, *Soft Matter* 2012, **8**, 6416–6429.
22 N. Oya, T. Ikezaki and N. Yoshie, *Polym. J.* 2013, **45**, 955–961.
23 F. Sordo, S.-J. Mougnier, N. Loureiro, F. Tournilhac and V. Michaud, *Macromolecules* 2015, **48**, 4394–4402.
24 J. Wu, L. H. Cai and D. A. Weitz, T, *Adv. Mater.* 2017, **29**, 1702616.
25 T. Kajita, A. Noro and Y. Matsushita, *Polymer* **2017**, *128*, 297–310.
26 P. F. Cao, B. Li, T. Hong, J. Townsend, Z. Qiang, K. Xing, K. D. Vogiatzis, Y. Wang, J. W. Mays, A. P. Sokolov and T. Saito, *Adv. Funct. Mater.* 2018, **28**, 1800741.
27 J. Kang, D. Son, G. J. N. Wang, Y. Liu, J. Lopez, Y. Kim, J. Y. Oh, T. Katsumata, J. Mun, Y. Lee, L. Jin, J. B. H. Tok and Z. Bao, *Adv. Mater.* 2018, **30**, 1706846.
28 Y. Yanagisawa, Y. Nan, K. Okuro and T. Aida, *Science* 2018, **359**, 72–76.
29 R. Tamate, K. Hashimoto, T. Horii, M. Hirasawa, X. Li, M. Shibayama and M. Watanabe, *Adv. Mater.* 2018, **20**, 1802792.
30 S. Burattini, B. W. Greenland, D. H. Merino, W. Weng, J. Seppala, H. M. Colquhoun, W. Mayes, M. E. Mackay, I. W.

Hamely and S. J. Rowan, *J. Am. Chem. Soc.* 2010, **132**, 12051–12058.
31 Q. Wang, J. L. Mynar, M. Yoshida, E. Lee, E. Lee, K. Okuro, K. Kinbara and T. Aida, *Nature* 2010, **463**, 339–343.
32 T. L. Sun, T. Kurokawa, S. Kuroda, A. Bin Ihsan, T. Akasaki, K. Sato, M. A. Haque, T. Nakajima and J. P. Gong, *Nature Mater.* 2013, **12**, 932–937.
33 A. Das, A. Sallat, F. Böhme, M. Suckow, D. Basu, S. Wießner, K. W. Stöckelhuber, B. Voit and G. Heinrich, *ACS Appl. Mater. Interfaces* 2015, **7**, 20623–20630.
34 N. Hohlbein, A. Shaaban, A. R. Bras, W. Pyckhout-Hintzen and A. M. Schmidt, *Phys. Chem. Chem. Phys.* 2015, **17**, 21005–21017.
35 C. Xu, L. Cao, B. Lin, X. Liang and Y. Chen, *ACS Appl. Mater. Interfaces* 2016, **8**, 17728–17737.
36 D. Wang, H. Zhang, B. Cheng, Z. Qian, W. Liu, N. Zhao and J. Xu, *J. Polym. Sci.: Part A: Polym. Chem.* 2016, **54**, 1357–1366.
37 Y. Miwa, J. Kurachi, Y. Kohbara and S. Kutsumizu, *Commun. Chem.* 2018, **1**, 5.
38 J. C. Lai, L. Li, D. P. Wang, M. H. Zhang, S. R. Mo, X. Wang, K. Y. Zeng, C. H. Li, Q. Jiang, X. Z. You and J. L. Zuo, *Nat. Commun.* 2018, **9**, 2725.
39 M. Suckow, A. Mordvinkin, M. Roy, N. K. Singha, G. Heinrich, B. Voit, K. Saalwächter and F. Böhme, *Macromolecules* 2018, **51**, 468–2479.
40 Y. Peng, Y. Yang, Q. Wu, S. Wang, G. Huang and J. Wu, *Polymer* 2018, **157**, 172–179.
41 Y. Peng, L. Zhao, C. Yang, Y. Yang, C. Song, Q. Wu, G. Huang and J. Wu, *J. Mater. Chem. A* 2018, **6**, 19066–19074.
42 Y. Miwa, K. Taira, J. Kurachi, T. Udagawa and S. Kutsumizu, *Nat. Commun.* 2019, **10**, 1828.
43 A. Mordvinkin, M. Suckow, F. Böhme, R. H. Colby, C. Creton and K. Saalwächter, *Macromolecules* 2019, **52**, 4169–4184.
44 M. Nakahata, Y. Takashima, H. Yamaguchi and A. Harada, *Nat. Commun.* 2011, **2**, 511.
45 T. Kakuta, Y. Takashima, T. Nakahara, M. Otsubo, H. Yamaguchi and A. Harada, *Adv. Mater.* 2013, **25**, 2849–2853.
46 M. Burnworth, L. Tang, J. R. Kumpfer, A. J. Duncan, F. L. Beyer, G. L. Fiore, S. J. Rowan and C. Weder, *Nature* 2011, **472**, 334–337.
47 G. Hong, H. Zhang, Y. Lin, Y. Chen, Y. Xu, W. Weng and H. Xia, *Macromolecules* 2013, **46**, 8649–8656.
48 D. Mozhdehi, S. Ayala, O. R. Cromwell and Z. Guan, *J. Am. Chem. Soc.* 2014, **136**, 16128–16131.
49 C. H. Li, C. Wang, C. Keplinger, J. L. Zuo, L. Jin, Y. Sun, P. Zheng, Y. Cao, F. Lissel, C. Linder, X. Z. You and Z. Bao, *Nat. Chem*. 2016, **8**, 618–624.
50 J. F. Mei, X. Y. Jia, J. C. Lai, Y. Sun, C. H. Li, J. H. Wu, Y. Cao, X. Z. You and Z. Bao, *Macromol. Rapid Commun.* 2016, **37**, 1667–1675.
51 D. P. Wang, J. C. Lai, H. Y. Lai, S. R. Mo, K. Y. Zeng, C. H. Li and J. L. Zuo, *Inorg. Chem.* 2018, **57**, 3232–3242.
52 L. Zhang, Z. Liu, X. Wu, Q. Guan, S. Chen, L. Sun, Y. Guo, S. Wang, J. Song, E. M. Jeffries, C. He, F.-L. Qing, X. Bao and Z. You, *Adv. Mater.* 2019, **31**, 1901402.
53 J. C. Lai, X. Y. Jia, D. P. Wang, Y. B. Deng, P. Zheng, C. H. Li, J. L. Zuo and Z. Bao, *Nat. Commun.* 2019, **10**, 1164.
54 S. Terryn, J. Brancart, D. Lefeber, G. Van Asssche and B. Vanderborght, *Sci. Robot.* 2017, **2**, 4268.
55 J. Li, L. Geng, G. Wang, H. Chu and H. Wei, *Chem. Mater.* 2017, **29**, 8932–8952.
56 T. P. Huynh, P. Sonar and H. Haick, *Adv. Mater.* **2017**, *29*, 1604973.
57 M. R. Tant, J. H. Song, G. L. Wilkes, J. Horrion and R. Jérôme, *Polymer* 1992, **33**, 1347–1358.
58 R. A. Register, M. Foucart, R. Jérôme, Y. S. Ding and S. L. Cooper, *Macromolecules* 1988, **21**, 1009–1015.
59 L. J. Fetters, W. W. Graessley, N. Hadjichristidis, A. D. Kiss, D. S. Pearson and L. B. Younghouse, *Macromolecules* 1988, **21**, 1644–1653.
60 L. N. Venkateshwaran, M. R. Tant, G. L. Wilkes, P. Charlier and R. Jérôme, *Macromolecules* 1992, **25**, 3996–4001.
61 M. R. Tant, L. N. Venkateshwaran, J. H. Song, R. Subramanian, G. L. Wilkes, P. Charlier and R. Jérôme, *Polymer* 1992, **33**, 1347–1358.
62 S. Maeda, Y. Harabuchi, Y. Osada, T. Taketsugu, K. Morokuma and K. Ohno, *GRRM*14, Version 14.01, 2014.
63 K. Ohno and S. Maeda, *Chem. Phys. Lett.* 2004, **384**, 277–282.
64 S. Maeda and K. Ohno, *J. Phys. Chem. A* 2005, **109**, 5742–5753.
65 K. Ohno and S. Maeda, *J. Phys. Chem. A* 2006, **110**, 8933–8941.
66 S. Maeda and K. Ohno, *J. Phys. Chem. A* 2007, **111**, 4527–4534.
67 Y. Zhao and D. G. Truhlar, *Theor. Chem. Acc.* 2008, **120**, 215–241.
68 M. J. Frisch et al., *Gaussian 09, Revision B.01*; Gaussian, Inc.: Wallingford CT, 2010.
69 D. J. Yarusso and S. L. Cooper, *Polymer* 1985, **26**, 371–378.
70 A. Eisenberg, B. Hird and R. B. Moore, *Macromolecules* 1990, **23**, 4098–4107.
71 L. J. Fetters, D. J. Lohse and R. H. Colby, In *Physical Properties of Polymers Handbook.* ed. Mark, J. E. AIP Press, New York, 1996, Chapter 24.
72 A. Abou Elfadl, R. Kahlau, A. Herrmann, V. N. Novikov and E. A. Rössler, *Macromolecules* 2010, **43**, 3340–3351.
73 J. G. Van Alsten, *Macromolecules* 1996, **29**, 2163–2168.
74 N. R. Tierney and R. A. Register, *Macromolecules* 2002, **35**, 2358–2364.
75 N. K. Tierney and R. A. Register, *Macromolecules* 2002, **35**, 6284–6290.
76 M. Tosaka, S. Murakami, S. Poompradub, S. Kohjiya, Y. Ikeda, S. Toki, I. Sics and B. S. Hsiao, *Macromolecules* 2004, **37**, 3299–3309.
77 L. Leibler, M. Rubinstein and R. H. Colby, *Macromolecules* 1991, **24**, 4701–4707.
78 R. H. Colby, X. Zheng, M. H. Rafailovich, J. Sokonov, D. G. Peiffer, S. A. Schwarz, Y. Strzhemechny and D. Nguyen, *Phys. Rev. Lett.* 1998, **18**, 3876–3879.
79 Q. Chen, S. Liang, S. Shiau and R. H. Colby, *ACS Macro Lett.* 2013, **2**, 970–974.
80 Q. Chen, C. Huang, R. A. Weiss and R. H. Colby, *Macromolecules* 2015, **48**, 1221–1230.
81 M. Ahmadi, L. D. G. Hawke, H. Goldansaz and E. van Ruymbeke, *Macromolecules* 2015, **48**, 7300–7310.
82 C. Huang, C. Wang, Q. Chen, R. H. Colby and R. A. Weiss, *Macromolecules* 2016, **49**, 3936–3947.
83 X. Cao, X. Yu, J. Qin and Q. Chen, *Macromolecules* 2019, **52**, 8771–8780.
84 M. Hofmann, A. Herrmann, A. Abou Elfadl, D. Kruk, M. Wohlfahrt and E. A. Rössler, *Macromolecules* 2012, **45**, 2390–2401.
85 R. P. Wool and K. M. O'Connor. *J. Appl. Phys.* 1981, **52**, 5953–5963.

We demonstrate the principle in the optimization of the molecular structure for the polyisoprene elastomer with dynamic ionic crosslinks to tune the mechanical and autonomous self-healing properties.